

Li-Ion Storage and Diffusivity in Sulfurized Polybutadiene Containing Covalently Bound Sulfur as a Polysulfide Shuttle-Free Cathode Material for Li–S Batteries

Sadananda Muduli,^[a] Marcel Boecker,^[b] Leon Prädel,^[b] Christof Neumann,^[c] Qian Du,^[a] and Michael R. Buchmeiser^{*[a, d]}

In this work, a new polymer has been explored as a cathode host for lithium-sulfur batteries (LSBs). Sulfurized polybutadiene materials were synthesized by a single-step, scalable, and easily tailored heat treatment method. The optimized synthesis process allows for high sulfur loadings of up to 50 wt%. Thermogravimetric analysis-mass spectrometry (TGA-MS) and X-ray photoelectron spectroscopy (XPS) studies confirm that the sulfur is covalently bound to the polymeric backbone, which overcomes the otherwise common capacity-fading polysulfide shuttle effect of lithium-sulfur (LSBs) batteries. The absence of free elemental sulfur in the synthesized active materials allows

for a stable capacity of up to 1200 mAhg⁻¹ at a rate of C/20. The porous polymer networks reduce the pulverization of the cathode during cycling, resulting in long-term cycling stability of 1500 continuous galvanostatic charge/discharge (GCD) cycles. Capacity contribution studies depict that at a scan rate of 1 mVs⁻¹, the sulfurized polybutadiene cathode-based cells have 65% capacitive and 35% diffusive contribution of the total charge stored. A comprehensive study on Li-ion storage with capacity contribution and diffusion studies of polysulfide shuttle-free sulfurized polybutadiene cathode material for LSBs is presented.

Introduction

The world's energy demand is rising continuously; consequently, intensive efforts are made to develop renewable energy and energy storage systems.^[1,2] Over the last two decades, Li-ion batteries have dominated the market for electric vehicles (EVs), electronic devices, and power backups, out-rivalling other secondary and primary battery systems.^[3,4] However, from an energy density and sustainability point of view, lithium-sulfur batteries (LSBs) are an effective alternative to meet the rising demand for batteries owing to the non-toxic, earth-abundant, and low cost of sulfur sources compared to other cathode materials.^[5,6] LSBs comprise a Li anode and a cathode based on sulfur or a sulfur-rich material. Sulfur has a

high theoretical capacity of 1675 mAh/g_{sulfur}^[7,8] which makes it attractive for replacing existing cathode materials like LiFePO₄, LiNMC, or LiCoO₂.^[7,9] From a safety point of view, the low operating potential of 2.1 V as compared to current high-voltage (>3.3 V) intercalation cathode materials^[10] might be advantageous; however, results in lower energy density. Also, LSBs still have some additional disadvantages to overcome. Those are the poor electrical conductivity of sulfur, pulverization of the cathode during continuous GCD cycling, the polysulfide shuttle effect, anode failure due to insoluble Li₂S coating, low sulfur utilization (<80%), low Coulombic efficiency, severe self-discharge, and short life cycle (<200),^[11-14] to name the most relevant ones. Consequently, many approaches involving tailored electrode architectures, active material modifications, interlayer-separator modifications, electrolyte additives, and cell activation methods have been designed and reported.^[5,7,12,15] 0D, 1D, and 2D conductive additives like carbon dots, CNTs, and graphenes helped in increasing conductivity.^[16-19] Further, electrode coating additives and 3D electrode architectures, i.e. carbon cloth or fibers as current collectors, contributed to an impeded pulverization of the cathode material during cycling.^[18,20,21] Such modifications in various ways improved the electrochemical performance of LSBs, yet did not completely suppress the polysulfide shuttle, which is one of the reasons why LSBs are still not available on the market.^[9,12,22,23] Several articles illustrate that porous carbon frameworks and MOF materials show a substantially reduced polysulfide shuttle effect; nonetheless, they suffer from complicated and expensive syntheses as well as limited sulfur loading and consequently have low capacity and energy density.^[22,24-26] In contrast, organosulfur composites have attracted attention as in these materials the sulfur is covalently bound to the

[a] S. Muduli, Q. Du, M. R. Buchmeiser
Institute of Polymer Chemistry, University of Stuttgart, Pfaffenwaldring 55,
D-70569 Stuttgart, Germany
E-mail: michael.buchmeiser@ipoc.uni-stuttgart.de

[b] M. Boecker, L. Prädel
Max Planck Institute for Polymer Research, Ackermannweg 10, D-55128
Mainz, Germany

[c] C. Neumann
Instituto of Physical Chemistry, Friedrich Schiller University Jena, Lessingstraße
10, D-07743 Jena, Germany

[d] M. R. Buchmeiser
German Institutes of Textile and Fiber Research (DITF) Denkendorf,
Koerschtastrasse 26, D-73770 Denkendorf, Germany

 Supporting information for this article is available on the WWW under
<https://doi.org/10.1002/batt.202400495>

 © 2024 The Authors. *Batteries & Supercaps* published by Wiley-VCH GmbH.
This is an open access article under the terms of the Creative Commons Attribution License, which permits use, distribution and reproduction in any medium, provided the original work is properly cited.

polymeric backbone, which turned out to be highly effective in reducing the polysulfide shuttle effect.^[14,27–30] However, the main challenge in these materials is to further increase the comparably low sulfur loading from typically 35–45 wt-% in order to increase their energy density.

Results and Discussion

Synthesis of Sulfurized Poly(Butadiene)s, Morphological and Structural Characterization

The synthesis of sulfurized poly(butadiene)s (SPBs) was accomplished in a tailored one-step thermal process (Scheme 1). Briefly, poly(butadiene) (PB) was mixed with excess sulfur and first heated to 300 °C, followed by heating to 400 °C, 450 °C and 500 °C to yield SPB-400, SPB-450, and SPB-500, respectively. Elemental analysis revealed a sulfur content of 48 wt-%, 50 wt-%, and 45 wt-% for SPB-400, SPB-450, and SPB-500, respectively (Table S1, Supporting Information).

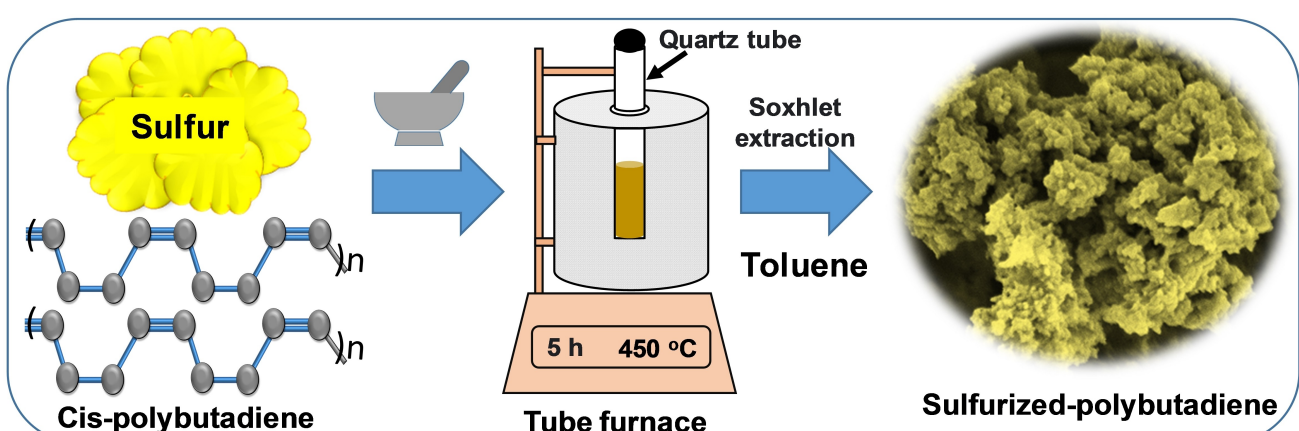
To study the morphological differences between the individual SPB cathode materials prepared at different temperatures, all SPBs were characterized by SEM (Figure 1(a–c)) and high-resolution TEM. SPB-400 (Figure 1a) agglomerated to secondary particles >1 μm in size with smaller primary particles (10–20 nm) as compared to SPB-450, in which 10–20 nm primary particles agglomerated to secondary particles ~0.5 μm in size (Figure 1b). SPB-500 (Figure 1c) had slightly larger primary particles (20–30 nm) as compared to SPB-450. EDX mapping for SPB-450 shown in Figure 1(d–f) reveals that the sulfur is uniformly distributed over the polymer backbone, confirming the effectiveness of the synthesis. High-resolution TEM images of SPB-400, SPB-450, and SPB-500 (Figure 1(g–i)) also confirmed that all composites consisted of primary nanoparticles 20–40 nm in diameter. The effect of synthesis temperature on particle size distribution and porosity of the synthesized material was additionally examined by N₂ adsorption-desorption experiments with P/P₀ values ranging from 1.0 to 0.1,^[31] showing type-II isotherms indicative for a nanoporous structure (Figure 2a). The specific surface areas of SPB-400, SPB-

450, and SPB-500 were 128, 138, and 194 m²g⁻¹, respectively (Table S1, Supporting Information). The pore size distribution curves of SPB-400, SPB-450, and SPB-500 are shown in Figure 2b and illustrate that the majority of the pores had diameters in the range of 1–5 nm. SPB-500 had more nanopores as compared to the other two materials due to the highest synthesis temperature, in line with the highest specific surface area. Unfortunately, high specific surface areas facilitate electrolyte decomposition, resulting in irreversible capacity loss;^[32–35] accordingly, SPB-500 showed a reduced cycling stability compared to SPB-450 (vide infra).

Generally, the presence of elemental sulfur (S₈) in a composite material results in polysulfide dissolution, which causes capacity fading and battery failure. Accordingly, all synthesized materials were characterized by XRD to investigate the purity of the materials. The XRD plots of SPB-400, SPB-450, and SPB-500 shown in Figure 2c do not reveal the presence of any elemental sulfur.^[36,37] Instead, all sulfur is covalently bound to the polymer.

In line with that, TGA-MS of SPB-450 (Figure 2d) revealed an initial 5% weight loss up to 350 °C corresponding to the loss of adsorbed moisture (*m/z*=18), whereas the absence of any sulfur fragments (S_x) further supports the absence of S₈. The second weight loss started above 350 °C and continued up to 1000 °C with a total weight loss of 45% under concomitant formation of S (*m/z*=32), CS (*m/z*=44), CS₂ (*m/z*=76), C₃H₂ (*m/z*=38), and C (*m/z*=12) fragments. This, on the one hand, nicely illustrates the thermal stability of the sulfurized polymer composite material up to 350 °C. On the other hand, the formation of the CS and CS₂ fragments provides further evidence for the formation of C–S bonds during composite synthesis.

The electronic states of the elements in the composite materials were scrutinized by XPS measurements (Figure 3). The survey spectrum of SPB-450 (Figure 3a) confirms the presence of S, C, and O and thus the purity of the material. The Si signals stem from the Si substrate that was used during XPS measurements. The deconvoluted S 2p spectrum (Figure 3b) shows two different spin-orbit splitted doublets at binding energies of 164.8 (S 2 p_{1/2}), 163.6 (S 2 p_{3/2}), and 162.4 (S 2 p_{1/2}), 161.2 eV (S 2



Scheme 1. Synthesis methodology of sulfurized-poly(butadiene)s.

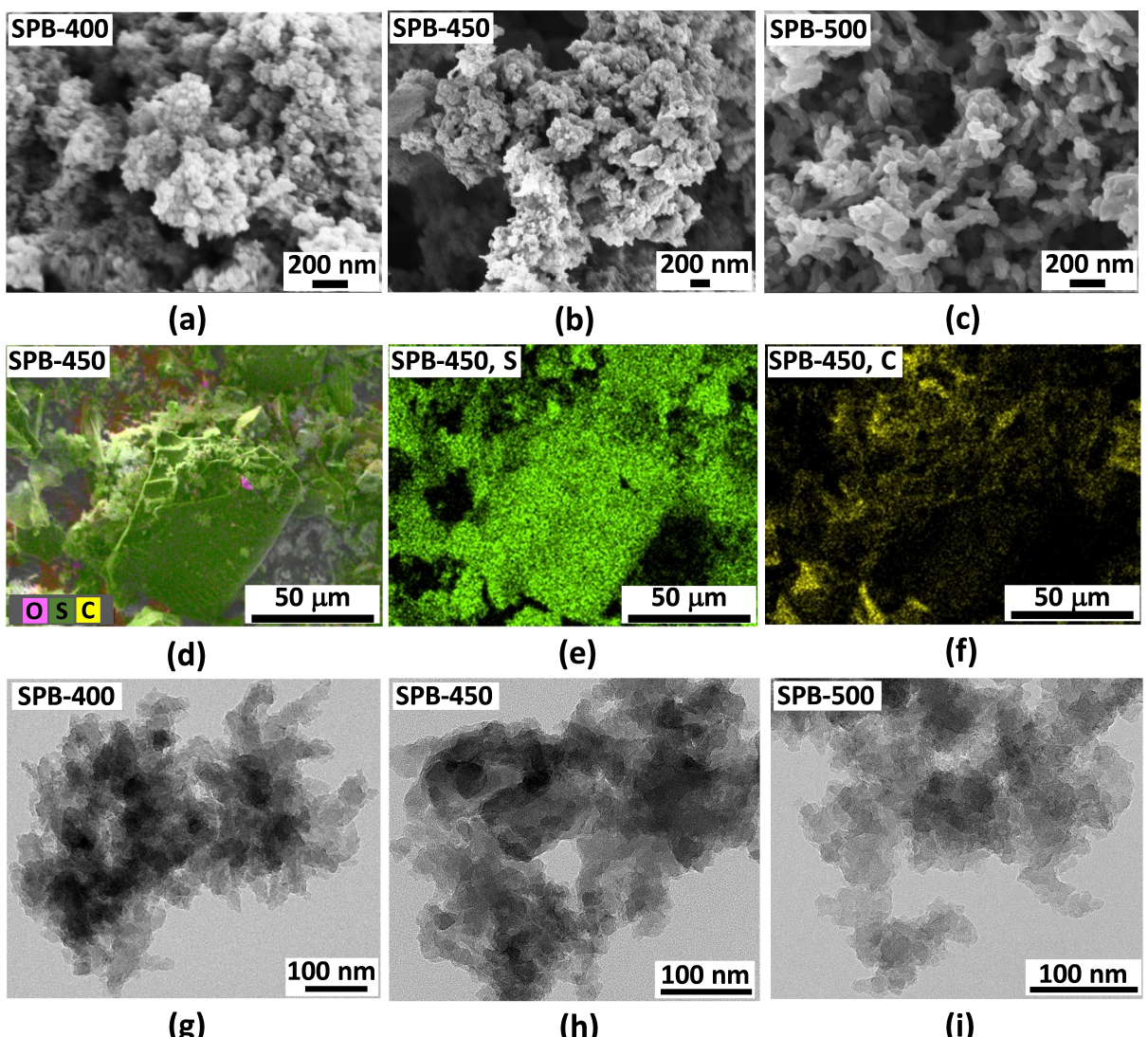


Figure 1. Morphological characterization. SEM images of (a) SPB-400, (b) SPB-450, (c) SPB-500; EDX analysis of SPB-450 (d) full mapping area, (e) S mapping, and (f) C mapping; TEM images of (g) SPB-400, (h) SPB-450, and (i) SPB-500.

$p_{3/2}$), corresponding to the C–S and C=S signals, respectively, indicative for a –2 oxidation state of sulfur in the composite materials.^[10,14] The absence of a peak for elemental sulfur in the deconvoluted S 2p spectra further confirms that all the sulfur atoms are covalently attached to the polymer backbone.^[10,38] Further, the deconvoluted C 1s spectrum (Figure 3c) endorses the presence of C–C, C–S/C=S, and C=O/C–O bonds at binding energies of 284.6, 286.9, and 288.4 eV, respectively.^[10,13] Similarly, the deconvoluted O 1s spectrum (Figure 3d) validates the presence of C=O and COO– bonds, confirming the formation of carbonyl and carboxylic groups in the composite materials. These functional groups were complementary and identified by Fourier-transform infrared (FT-IR) spectroscopy as presented in Figure S1a, Supporting Information. The solid-state ^{13}C NMR spectrum of SPB-450 (Figure S1b, Supporting Information) reveals a weak signal around $\delta = 45$ ppm attributable to the remaining aliphatic carbons of the SPB materials. The most intense broad peak centered at $\delta = 137$ ppm corresponds to

aromatized carbon atoms bound to sulfur, i.e. to thiophene-type sp^2 carbons, which form during the high-temperature sulfurization process.^[39,40] Finally, a broad peak in the range of $\delta = 200\text{--}240$ ppm suggests the presence of thiocarbonyl groups. Results are in line with the XPS and FT-IR data (Figure S1, Supporting Information).

Electrochemical Characterization

Li–S coin cells were fabricated using the different SPB cathode materials and their electrochemical performance was studied. Firstly, cyclic voltammetry was performed to identify the active potential window of the active material, which was found to be between 0.1 and 3.0 V (Figure 4a). The CV plot recorded at a scan rate of 0.1 mVs^{-1} showed in the first cycle two cathodic reduction peaks corresponding to a reduction of S_8 to Li_2S_x at 1.64 V and then to $\text{Li}_2\text{S}_2/\text{Li}_2\text{S}$ at 0.68 V, whereas the anodic

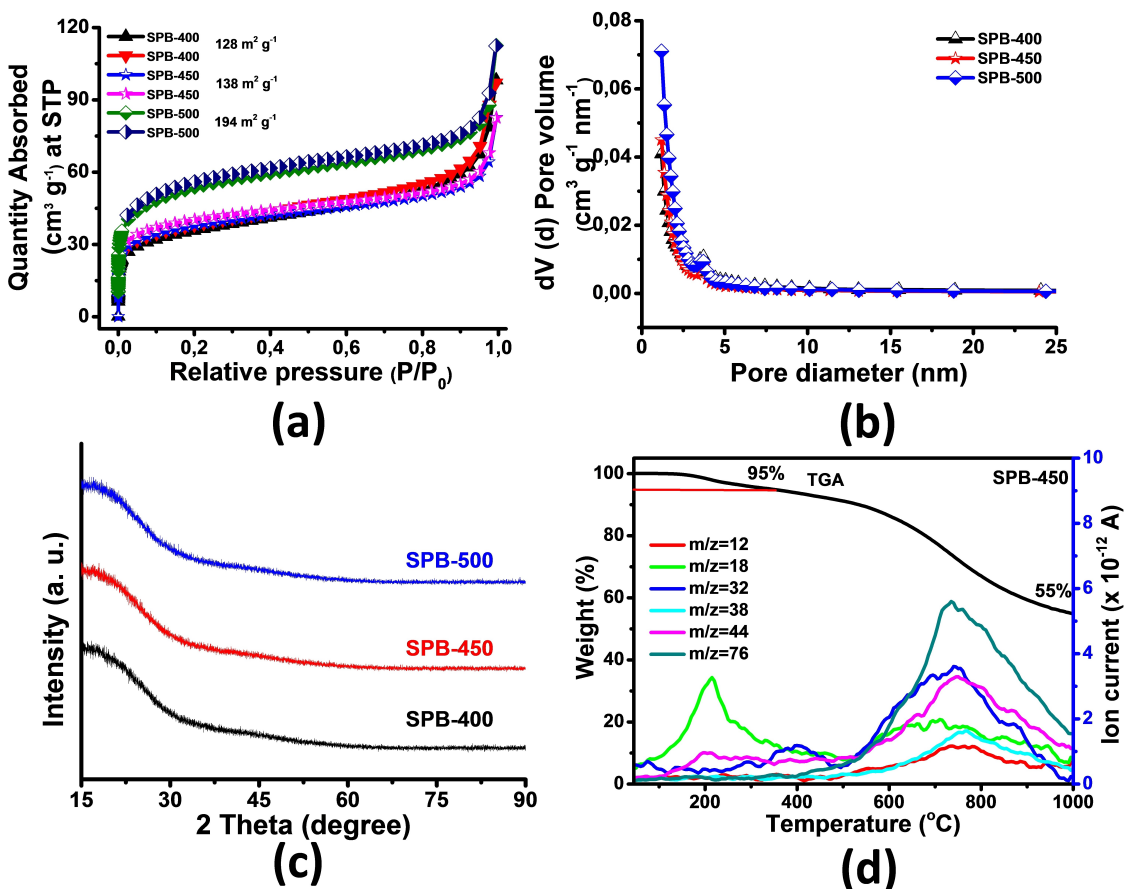


Figure 2. Structural characterization. (a) N₂-adsorption-desorption curves and (b) pore size distributions; (c) XRD of SPB-400, SPB-450, and SPB-500; (d) TGA-MS of SPB-450.

oxidation peaks depict conversion of lower order to higher order sulfur species at initially 1.9 V and then at 2.35 V.^[11,14,38,41]

In the following cycles, both the reduction and oxidation peaks shifted and in the fifth CV cycle, a single broad peak was observed for both anodic and cathodic scans, illustrating the effectively reversible conversion of lower to higher-order sulfur species and vice-versa. Figure 4b presents the first three formation cycles of the cells at a C/30 rate, which revealed an irreversible discharge capacity of 2500 mAh g⁻¹ during the first discharge, ascribed to the initial reduction of the polymer network structure, typical for sulfurized polymers.^[10,13,14,29,38,42] The achievable capacity in the sixth discharge cycle was 1350 mAh g⁻¹. Such high capacity at C/30 rate clearly illustrates the effectiveness of the sulfurized polybutadiene as cathode material in the Li–S batteries.

Next, charge storage studies were carried out for SPB-400, SPB-450, and SPB-500 applying the GCD method at a C/20 rate (Figure 4c). The achievable capacity values were 1200, 1250, and 1350 mAh g⁻¹ for SPB-450, SPB-400, and SPB-500, respectively. The observed capacity trend is in line with the sulfur loading of 50, 48, and 45 wt % in SPB-450, SPB-400, and SPB-500, respectively. Clearly, the material with the lowest S-content showed the highest sulfur utilization using the same tap-density of the electrodes. However, since SPB-450-based cells showed a higher nominal voltage than other active materials and had the

highest sulfur content, directing to the improved energy density of batteries based on this cathode material, all further electrochemical characterization focused on SPB-450-based Li–S cells. Figure 4d presents the GCD curves for C-rates of C/20, C/10, C/5, C/2, and 1 C. The corresponding achievable capacities were 1200, 1040, 840, 635, and 515 mAh g⁻¹ respectively (Figure 4d). Such promising capacity at high C-rates is a result of the covalently bound sulfur that allows for an efficient Li⁺ ion insertion/deinsertion without polysulfide dissolution. We attribute the lower achievable capacity at, e.g. 1 C as compared to C/20 to an incomplete addressing of all sulfur as a result of diffusion-limited processes.

Kinetic Studies

Kinetics studies were carried out to understand the charge storage mechanism of SPB-450-based electrodes. Initially, CV measurements were carried out at 0.1–1.0 mV s⁻¹ at an interval of 1 mV s⁻¹ (Figure 5a); the corresponding plot of peak current versus scan rate is presented in Figure 5b.

The fitted curves deviate from the actual data points, illustrating the involvement of both diffusive and capacitive charge storage mechanisms. Stored charge contributions were identified using both the "Power law"^[43–45] and "The Trasatti

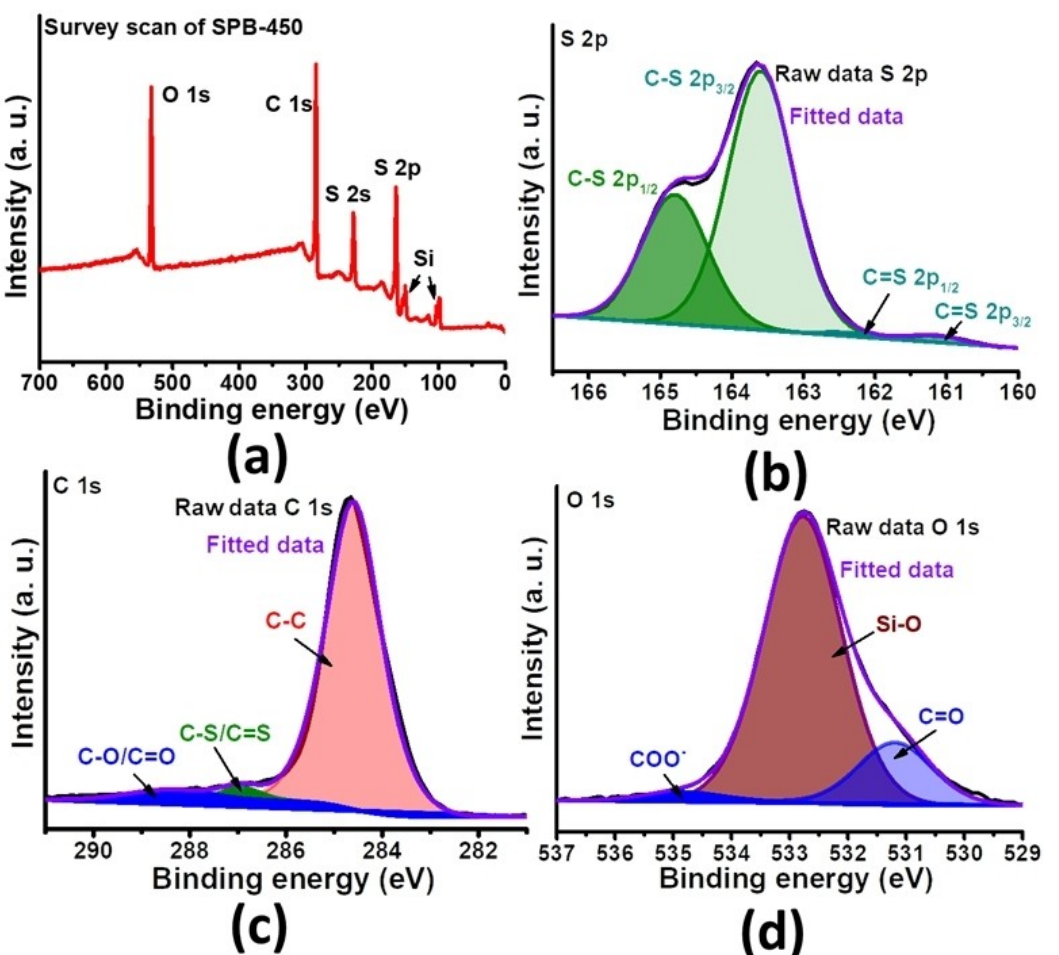


Figure 3. XPS analysis of SPB-450. (a) Survey spectrum, high-resolution (b) S 2p, (c) C 1s, and (d) O 1s spectra.

method".^[45–48] "Power law" defines the CV currents (i) to be related to the scan rate (v) by the following equation

$$i = av^b$$

in which a and b are adjustable parameters. The b -values define the charge storage process as diffusive for $b=0.5$ and capacitive for $b=1.0$.^[43,44,49] Here, the b -values were estimated from the plot of $\log(i)$ vs $\log(v)$ as 0.9888, 0.9021, 0.6743, 0.5839, and 0.9497 for 0.5, 1.0, 1.5, 2.25, and 2.4 V, respectively (Figure 5c). At 1.5 and 2.25 V (Figure 5c) the fitted line deviates from those at other voltage values due to slightly shifted positions of the redox peaks (Figure 5a) resulting in b values of 0.67 and 0.58. Such b -values confirm the involvement of both capacitive and diffusive charge storage phenomena. To calculate the percentage of diffusive and capacitive components "The Trasatti method" was employed,^[43,44] which states that the total current ($i(v)$) is the sum of the capacitive (S_1v) and diffusive currents ($S_2v^{0.5}$) for a specific potential; the equation is expressed as

$$i(v) = S_1v + S_2v^{0.5}$$

$$\Rightarrow \frac{i(v)}{v^{0.5}} = S_1v^{0.5} + S_2$$

In these equations, S_1 and S_2 are adjustable parameters, whose values are calculated from the slope and intercept of the plot of $i(v)/v^{0.5}$ versus $v^{0.5}$ to estimate the charge storage contributions.^[43,44] Figure 5d shows that at a 1 mV s^{-1} scan rate, the SPB-450 cathode-based cells had 65% capacitive and 35% diffusive contribution for total stored charge. The contribution percentages for different scan rates are presented in Figure 5e. With increasing scan rates an increase in capacitive contribution was observed due to the fast kinetics of the Li^+ ion, i.e. at high scan rates the capacitive and at low scan rates the diffusive components are prominent. Further, the diffusion of Li^+ ions in an SPB-450 electrode was examined by the galvanostatic intermittent titration technique (GITT) method (Figure 6). Prior to GITT measurements, the coin cells were activated using ten formation cycles at $C/20$ rate and recharged at the end of the last cycle. A galvanostatic current of $C/10$ rate was applied for 20 minutes (pulse duration, τ) followed by 60 minutes OCV to measure the GITT of the cell. The voltage profile is shown in Figure 6a.

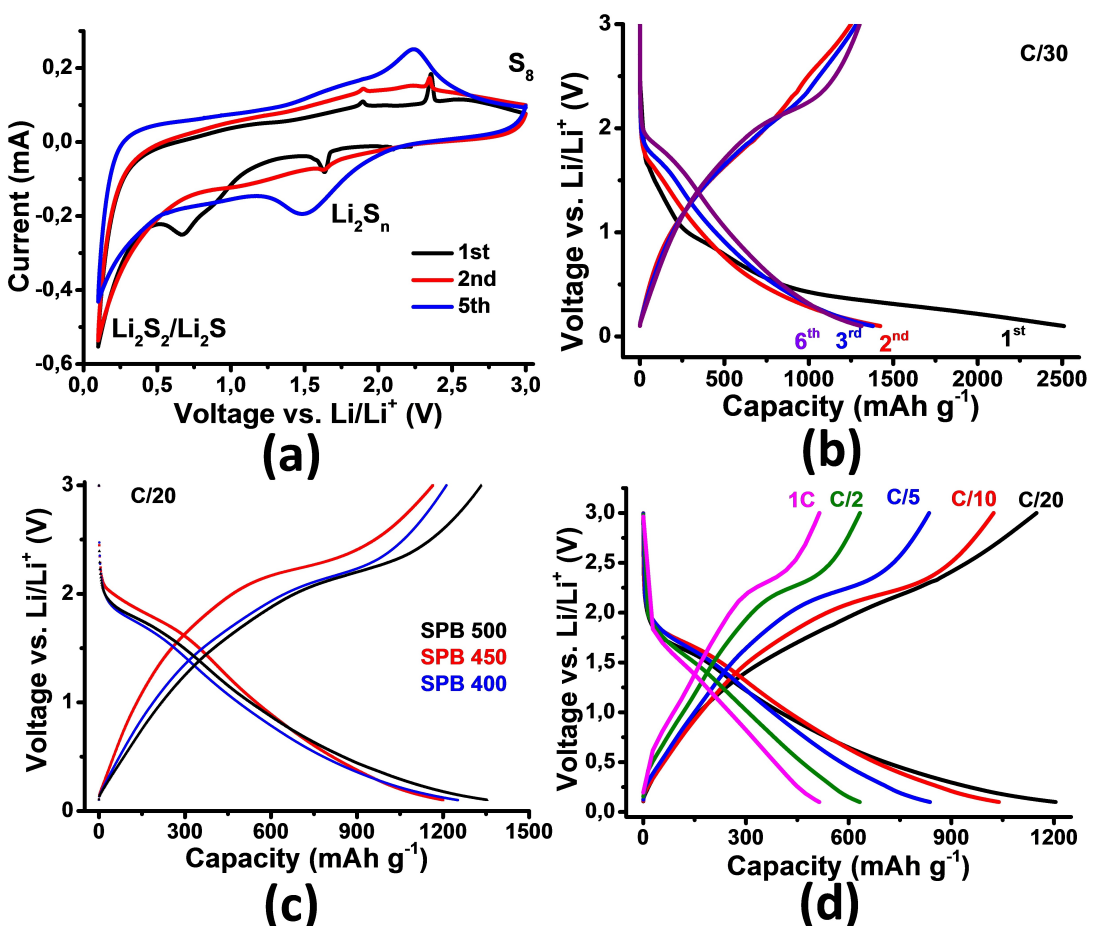


Figure 4. Electrochemical characterization. (a) Cyclic voltammogram, (b) initial GCD cycles at C/30 C-rate, (c) voltage profile plot of SPB-400, SPB-450, SPB-500 at C/20, and (d) voltage profile plot of SPB-450-based cells at various current densities.

The curve displays a pair of plateaus during discharge and charge, which are in accordance with the GCD and CV results presented in Figures 4d and 5a, respectively. Figure 6b presents the current step diagram at 0.8 V during lithiation. The solid-state diffusion coefficients of the Li-ion (D_{Li}) i.e. insertion/de-insertion of Li⁺ ion inside the electrode material during lithiation and delithiation were calculated using the "Weppner Huggins equation"^[49–52]

$$D_{Li} = \frac{4}{\pi \tau} \left(\frac{mV_m}{MS} \right)^2 \left(\frac{\Delta E_s}{\Delta E_t} \right)^2$$

in which m is the mass loading (g), M is the molecular weight, V_m is the molar volume, τ is the pulse duration, S is the area of the electrode, ΔE_s is the steady-state voltage change (V), and ΔE_t is the transient voltage change (V). The diffusion coefficient values for lithiation and delithiation are presented in Figures 6c and d. These plots illustrate that during discharge the diffusion coefficient initially increases to 1.2 V and then slowly decreases due to the formation of larger amounts of Li₂S/Li₂S₂. During charging, the diffusion coefficient decreases continuously due to the formation of sulfides. The diffusion coefficients are in good agreement with the reported literature.^[38,42]

C-Rate and Cycling Stability Studies

For potential practical use, C-rate and long-term cycling stability studies were carried out with SPB-450 cathode-based cells. The C-rate test (Figure 7a) was started with C/20 and then increased stepwise to C/10, C/5, C/2, 1 C, 2 C and, finally, to 3 C and then again decreased stepwise to C/10. Capacity values were almost fully restored after 70 GCD cycles. Comparative C-rate plots for SPB-400, SPB-450, and SPB-500 are presented in Figure S2, Supporting Information, and show that all three composite materials retain stable capacity after varying the applied current densities.

To determine the long-term cycling stability of SPB, cycling studies were carried out at a C/2 rate using an SPB-450-based cell (Figure 7b). Cells proved sufficiently stable for 1500 continuous GCD cycles with 58% of capacity retention. The cycling stability study for all three synthesized cathode materials (Figure S3, Supporting Information) revealed that SPB-500 had the lowest stability while SPB-450 was the most stable cathode material, as compared to SPB-400. We tentatively attribute the lower stability of SPB-500 to a larger content of micropores (<2 nm) as reflected by the higher specific surface area (Table S1, Supporting Information), facilitating electrolyte decomposition and irreversible capacity loss. This is supported

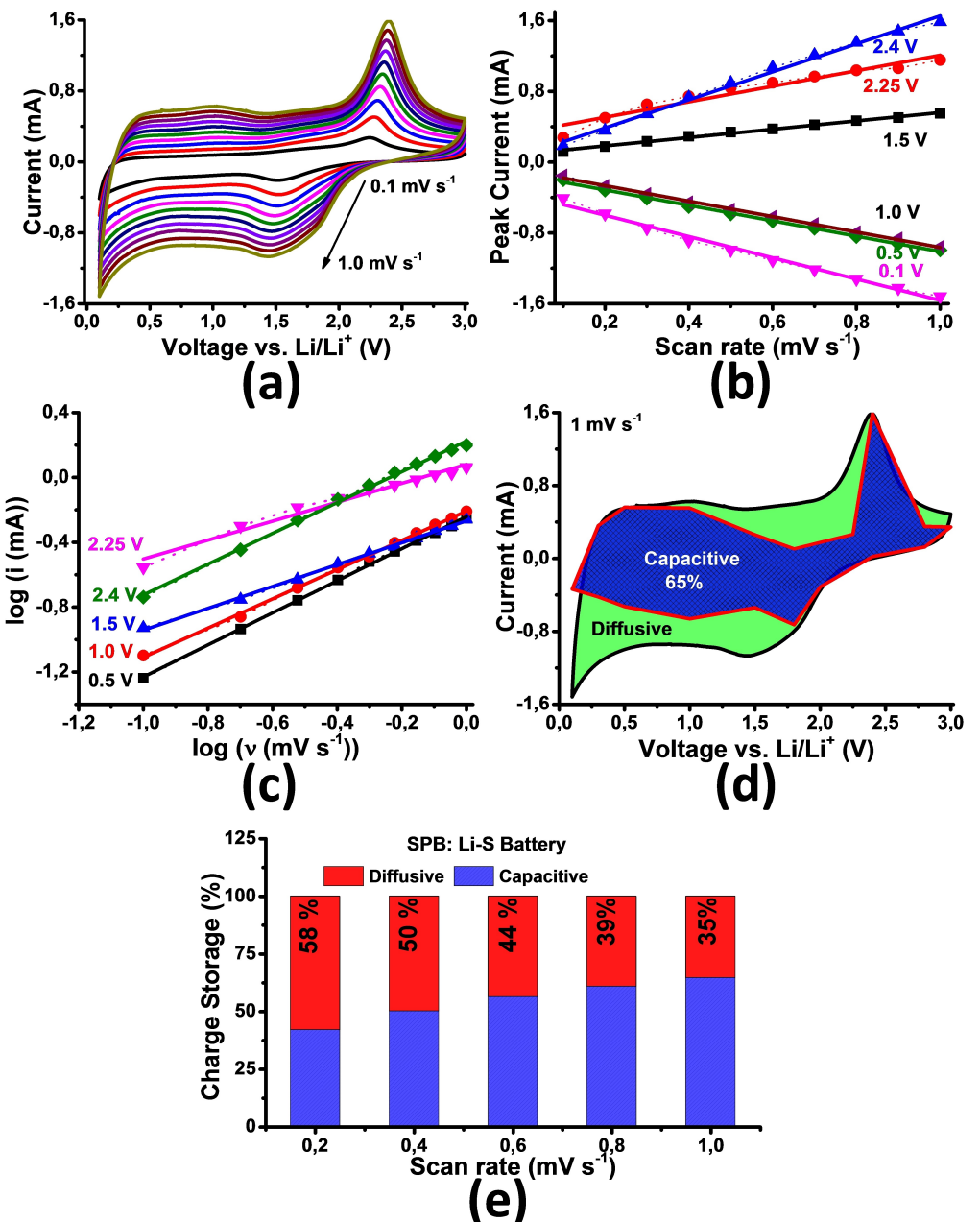


Figure 5. Capacitive and diffusive charge storage study. (a) CVs at various scan rates, (b) peak current vs scan rate plot, (c) log current vs log scan plot, (d) capacitive and diffusive plot for 1 mVs⁻¹, and (e) capacitive and diffusive percentage plot for various scan rates.

by many studies.^[32,33,35] Also, smaller particle sizes enhance the electrochemical performance, while less agglomerated nanoparticles with high specific surface areas are more susceptible to surface reactions and particle dissolution in the electrolyte, resulting in lower cycling stability. Also, high specific surface area materials based on larger nanoparticles give rise to larger local current density gradients and thus non-uniform potential polarization effects.^[32,33,35] Accordingly, SPB-500 having the highest specific surface area performs least stable in long-term cycling stability tests. The promising stable long life of SPB-450 with >98% Coulombic efficiency after 1500 cycles is attributed to a highly reversible conversion between polymer-bound short and long-chain polysulfides. The finding that SPB-450-based

composite electrodes are stable for 1500 GDC cycles whereas SPB-400 and SPB-500-based composite electrodes are only stable up to 600 and 400 GCD cycles, respectively (Figure S3, Supporting Information), may also tentatively be attributed to an optimum channeling of the electrolyte ions in SPB-450. The initial capacity fading till 300 cycles is attributed to the formation of a polymeric solid electrolyte interface (SEI) in an FEC-based electrolyte, whose thickness increases during lithiation to an optimum point due to the decomposition of the electrolyte solvent.^[53,54] Moreover, synergistic effects between porosity and specific surface area may explain the negligible polysulfide shuttle effect that reduces any non-conducting Li₂-Li₂S₂ coating on the Li anode, resulting in the observed long-

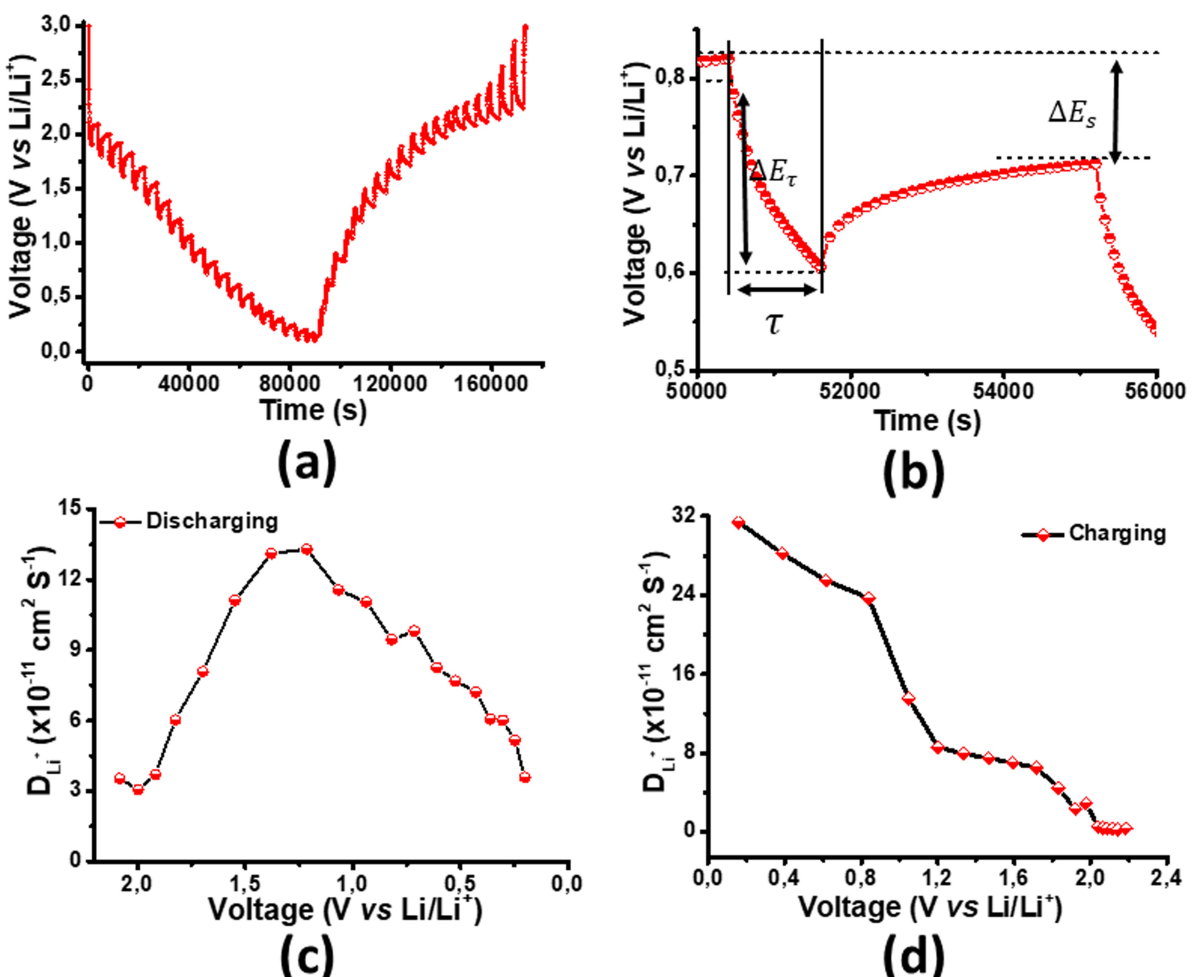


Figure 6. Diffusion study of SPB-450. (a) GITT plot, (b) current step vs time diagram at 0.8 V, (c and d) calculated diffusion coefficient during lithiation and delithiation.

term cycling stability. However, such an effect so far lacks hard proof. To further support this interpretation, impedance studies were carried out after 1500 GCD cycles with an SPB-450-based cathode (Figure 7c-d). In the high-frequency region, the Nyquist plot shows a small semicircle (only before cycling), corresponding to the electrode and double-layer interfacial impedance while the next large semicircle is attributed to the charge transfer resistance of sulfur intermediates without any sulfur or Li₂S_x dissolution. The Nyquist plots reveal that prior to cycling the cell had a solution resistance (R_s) of 1.4 Ω and a charge-transfer resistance (R_{ct}) of 22 Ω, while after cycling R_s and R_{ct} increased only moderately to 7 Ω and 40 Ω, respectively. Such low R_{ct} values point towards an efficient interaction of the electrolyte with the porous polymer network and high sulfur utilization, resulting in high electrochemical stability. By contrast, SPB-400 and SPB-500 cells show R_s values of 10 and 3 Ω and R_{ct} values of 40 and 30 Ω, respectively, before cycling. The R_s values increased to 12 and 5 Ω while the R_{ct} values increased to 60 and 80 Ω, respectively, after cycling, (Figure S4, Supporting Information). These higher R_s and R_{ct} values are in line with the lower cycling stability of SPB-400 cells compared to SPB-450 cells.

Post-Mortem Analyses

To investigate any structural changes after cycling, *post-mortem* analyses using SEM, XRD, and XPS were carried out on an SPB-450-based cell. After the cycling stability test over 1500 GCD cycles, the cell was fully charged and then de cramped inside an Ar-filled glove box. The disassembled cell (Figure 8a) did not show any stripping of active material. SEM (Figure 8b) revealed no agglomeration of the SPB-450 particles into large bulk particles even after 1500 GCD cycles, thereby maintaining the morphology of the pristine active materials. XRD (Figure 8c) showed only the Cu signals of the Cu-current collector and less intense carbon peaks of the conductive C-65 additive.^[55,56]

The absence of any signals for elemental sulfur in the XRD pattern even after 1500 GCD cycles confirms high reversibility of sulfur incorporation into the sulfurized polybutadiene upon charging, allowing for a cycle-stable, virtually polysulfide shuttle-free cathode material.^[36,37] Further *ex-situ* XPS of the cathodes after cycling (Figure 8b), as presented in Figure 8d, e, reveal the presence of polysulfides (Li₂S_x) in the S 2p and Li 1s spectrum, thereby confirming the formation of some inactive Li₂S/Li₂S₂ on the cathode side. As the cycling stability study

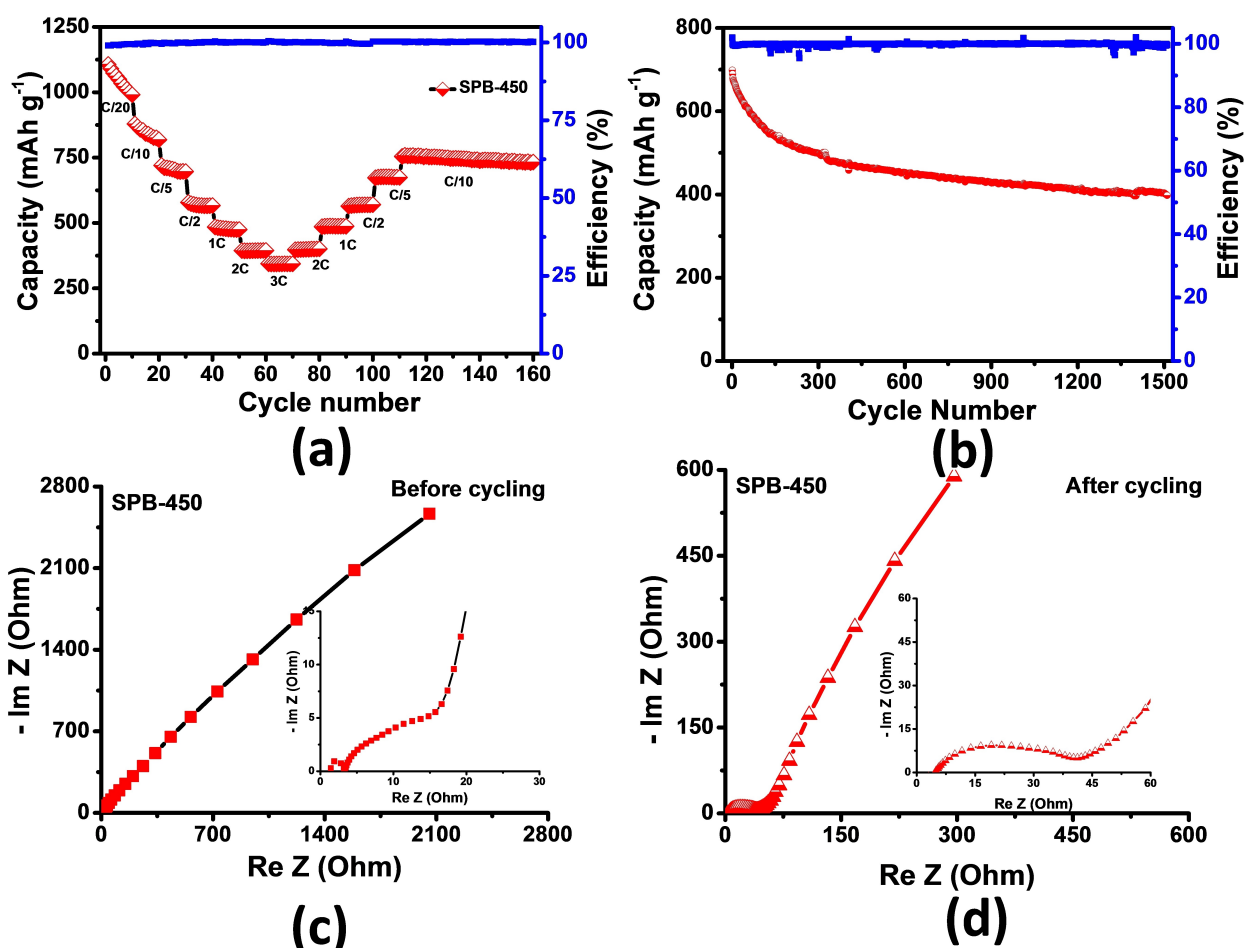


Figure 7. Electrochemical studies of SPB-450; (a) C-rate study, (b) cycling stability study at C/2 C-rate, (c and d) Nyquist plot before and after 1500 GCD cycling, (inserts represent the high-frequency parts of the Nyquist plots).

(Figure 7b) revealed that cells retained 58% capacity after continuous 1500 GCD cycles, only minor amounts of Li₂S/Li₂S₂ can be present in the cathode after cycling, suggesting highly reversible Li₂S and Li₂S₂ formation/reoxidation. Such outstanding electrochemical performance is a result of the effective coating of active material to the current collector, an efficient electrolyte interaction with the porous polymer network, and maximum sulfur utilization without any significant polysulfide shuttle effect. Finally, elemental analysis of SPB-450 after deep discharge at 0.1 V confirmed the presence of ~20 wt-% sulfur in the electrode material. This corresponds to approximately one sulfur atom per eight carbons, i.e. per two repeat units of poly(butadiene). In view of the 50 wt-% sulfur content in pristine SPB-450, an average sulfur chain length in the C–S_x–C moieties of x~4 can be calculated for this cathode material, which is in line with other sulfurized polymers such as sulfurized poly(acrylonitrile) (SPAN).^[57,58] As in SPAN, the polymer-C–S–Li⁺ sites in discharged SPB allow for the observed highly reversible incorporation of sulfur into the cathode material upon recharge.

Conclusions

Novel cathode materials have been synthesized from an easily accessible progenitor by a tailored thermal process. The scalable and easy synthesis offers access to cathode materials for LSBs containing up to 50 wt-% sulfur. The sulfur is covalently bound to the polymer as confirmed by TGA-MS, XRD, and XPS studies. The absence of any free elemental sulfur in the active materials provides a stable capacity of up to 1200 mAh g⁻¹ at a C/20 rate. Capacity contribution studies depict that at a scan rate of 1 mV s⁻¹, the sulfurized polybutadiene cathode-based cells have 65% capacitive and 35% diffusive contribution of the total charge stored. The porous polymer network reduces pulverization of the cathode material and is also key to a long-term cycling stability over 1500 continuous GCD cycles. Post-mortem analysis confirmed the presence of minor amounts of Li₂S/Li₂S₂ after continuous 1500 GCD cycles, suggesting highly reversible Li₂S and Li₂S₂ formation/reoxidation. The straightforward synthesis, the good availability of the starting material together with the promising charge storage and long-term cycling stability of SPB-450 cathode material render it promising for practical use. Finally, this work also provides a fundamental

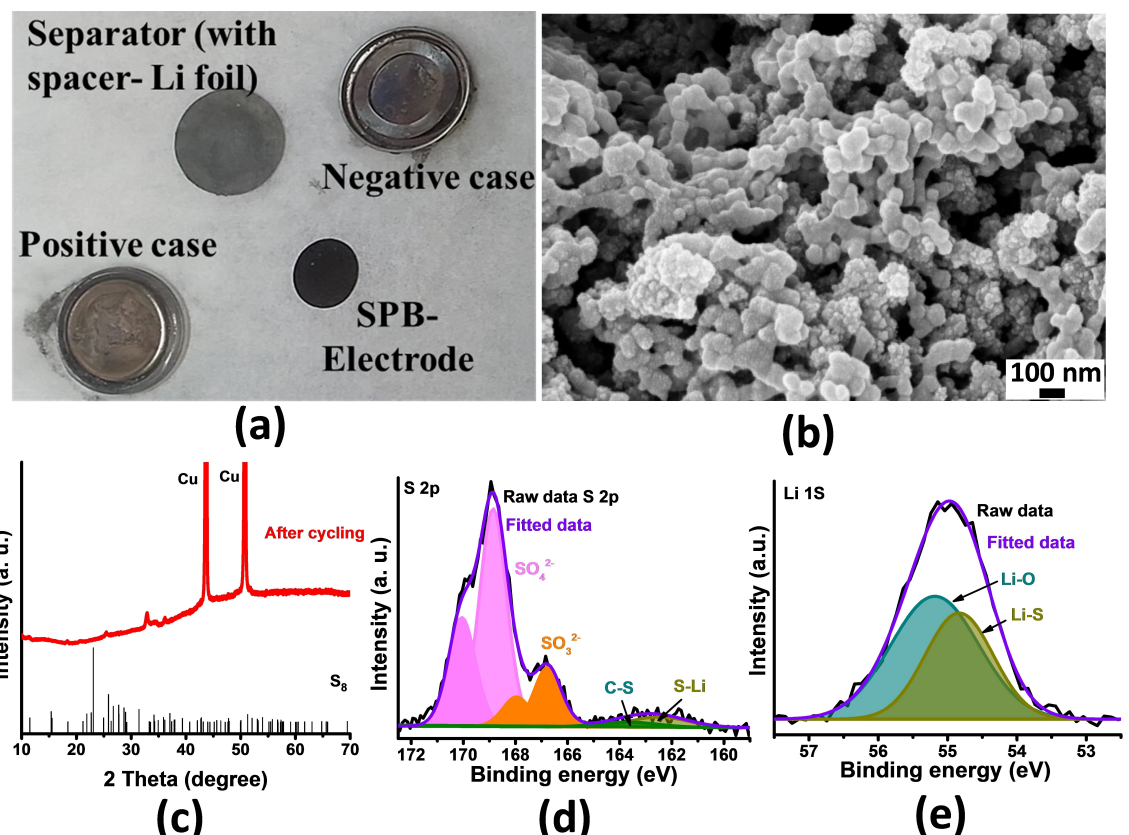


Figure 8. Post-mortem analysis of an SPB-450 cell after 1500 cycles. (a) Disassembled cell, (b) SEM, (c) XRD, and (d and e) high-resolution S 2p and Li 1s XPS spectrum.

understanding of Li^+ storage in these materials from capacity contribution and diffusion studies.

Experimental

Material Synthesis

Sulfurized-polybutadienes (SPBs) were synthesized by a simple high-temperature treatment method. Sulfur and *cis*-polybutadiene ($M_w = 470,000 \text{ g/mol}$, $D=2.7$, Sigma Aldrich, Germany) were mixed in a weight ratio of 20:1 (20 g and 1 g, respectively) and the mixture was placed in a quartz tube. The mixture was pre-activated at 200°C for 3 hours, then the reaction was completed at 400°C, 450°C and 500°C, respectively, for 5 hours using a high-temperature tube furnace (Nabertherm, Germany) under an N_2 atmosphere. The corresponding sulfurized materials are termed SPB-400, SPB-450, and SPB-500, respectively. After heat treatment, the materials were cooled to room temperature and collected. Excess unreacted sulfur was removed by Soxhlet extraction using toluene for 70 hours. The pure materials were vacuum-dried and sieved through 63 μm sieves and labeled as SPB-500.

Physical Characterization

Elemental analyses were carried out at the Institute of Inorganic Chemistry, University of Stuttgart, on a Vario MicroCube (Elementar Analysensysteme GmbH) at 1100°C against the pestanal standards Thiram (Sigma-Aldrich) and sulfanilamide (Elementar Analysensys-

teme GmbH). Field emission scanning electron microscopy (FE-SEM) and energy-dispersive X-ray (EDX) analysis was carried out on a ZEISS Auriga-FIB instrument. A ThermoFisher Spectra 300 machine was used for transmission electron microscopy (TEM) at 300 kV by bright field imaging. The TEM was equipped with a high-brightness Schottky Field Emission Gun (X-FEG). X-ray diffraction (XRD) patterns were measured on a D8ADVANCE machine from Bruker AXS, UK, in the 2 θ range of 15–90° using $\text{Cu K}\alpha$ ($\lambda=1.5418 \text{ \AA}$) radiation. TGA and MS measurements were carried out in a temperature range of 45–1000°C on a Q500 TGA (TA-Instruments) and on a QMS 403C Aëlos® (Netzsch instrument), respectively, applying a heating rate of 10 K/min under a He atmosphere. Specific surface areas and pore size distributions were determined by N_2 -adsorption-desorption measurements on a Quantachrome Autosorb IQ-MP-MP-MP instrument at 77 K using the Brunauer–Emmett–Teller (BET) method. FT-IR measurements were conducted on a Bruker ALPHA instrument, Germany. Solid state nuclear magnetic resonance (SS-NMR) measurements were carried out at 8 kHz on a Bruker Avance III 400 WB spectrometer. XPS measurements were carried out on a Kratos Axis Ultra DLD imaging photoelectron spectrometer with a monochromated $\text{Al K}\alpha$ source operating at a 10 mA emission current and a 15 kV voltage bias in a UHV chamber with a base pressure of approx. $1\times 10^{-10} \text{ mbar}$. The binding energy was calibrated vs. C 1s (284.6 eV), and the Origin 9.0 software with the Gaussian function was used for deconvolution of the XP spectra.

Cell Fabrication and Electrochemical Characterization

Composite electrodes were prepared by coating a slurry of the active material on carbon-coated Cu-foil using doctor blading. The slurry was prepared by mixing the corresponding SPB, carbon black (Sigma-Aldrich) and poly(vinylidene difluoride) (PVDF, Sigma-Aldrich) in a 70:15:15 weight-ratio using *N*-methylpyrrolidone (NMP) as solvent. After vacuum drying at 60 °C for 24 hours, disc-shaped electrodes 10 mm in diameter, having a tap density of ~2.5–3.0 mg, were punched out. Capacity calculations are based on the amount of sulfur. Li–S coin cells were fabricated from the prepared electrodes using a Li sheet as a reference counter electrode. Cells were fabricated inside a glove box using 1 M LiPF₆ in ethylene carbonate (EC): diethylene carbonate (DEC, 1:1% v/v) with 10 wt % fluoroethylene carbonate (FEC, Sigma-Aldrich) as electrolyte and one GF/C glass microfiber Whatman separator having 1.2 μm pore size. After OCV over a minimum of 12 hours, cells were connected to a Biologic VMP3 instrument for electrochemical measurements including cyclic voltammetry (CV), galvanostatic charge/discharge (GCD), electrochemical impedance spectroscopy (EIS) and C-rate measurements, galvanostatic intermittent titration technique (GITT), and cycling stability. All electrochemical measurements were carried out in a potential window of 0.1–3.0 V; the EIS studies were done in a frequency range of 10 mHz–1 MHz with a voltage amplitude of 10 mV.

Post-Mortem Analysis

For XRD, XPS, and SEM analysis, a long-term cycled cell was fully charged to 3 V and then unsealed inside an Ar-filled glove box. The electrode was cleaned properly with dimethyl carbonate to remove all contaminants and dried at 60 °C for 24 hours.

To determine the sulfur content of a discharged cell, a cell was run for 50 GCDs and then deep discharged to 0.1 V at a C/20 rate. Next, the cell was unsealed inside an Ar-filled glove box and the electrode was cleaned properly with dimethyl carbonate. Then the electrode was sonicated in dimethyl formamide for a few hours, the black mass was collected and washed with diethyl ether several times. After drying, the material was subjected to elemental analysis.

Author Contributions

Sadananda Muduli: conceptualization, methodology, formal analysis and experiments, data curation, writing – reviewing, and editing of the original manuscript. **Qian Du:** conceptualization. **Michael R. Buchmeiser:** conceptualization, data validation, supervision, methodology, writing – reviewing- and editing, funding acquisition. **Leon Prädel, Marcel Boecker:** XPS measurements. **Christof Neumann:** analysis of the XPS spectra.

Acknowledgements

We acknowledge Ms. Barbara Förtsch for elemental analyses, Mr. Vincent Gramm for BET measurements, as well as Ms Nagme Ay and Ms. Ines Lauerwald, all University of Stuttgart, for XRD measurements. We thank Ulrich Hageroth and Mr. Volker Bauch, German Institutes of Textile and Fiber Research (DITF) Denkendorf, for helping with SEM and TGA-MS measurements. We express thanks to Dr. Marie-Louise Lemloh, Dr. Florian Kauff-

man, and Mr. Michael Rolf Schweikert of the Advanced Materials Innovation and Characterization (AMICA) network at the University of Stuttgart for TEM measurement. We also thank PD Dr. Michael Dyballa, Institute of Technical Chemistry, University of Stuttgart, for recording the ¹³C NMR CP-MAS spectra. Finally, we acknowledge financial support within the KovaLiS project funded by the Federal Ministry of Education and Research (BMBF), Germany, grant no 03XP0576B. Open Access funding enabled and organized by Projekt DEAL.

Conflict of Interests

The authors declare no conflicts of interest.

Data Availability Statement

The data that support the findings of this study are available from the corresponding author upon reasonable request.

Keywords: Sulfurized polybutadiene; • Covalently bound sulfur; • Cathodes; • Li–S batteries

- [1] M. Büchs, N. Cass, C. Mullen, K. Lucas, D. Ivanova, *Nat. Energy* **2023**, 8, 758–769.
- [2] L. J. Sonter, M. C. Dade, J. E. M. Watson, R. K. Valenta, *Nat. Commun.* **2020**, 11, 4174.
- [3] J. Sun, T. Wang, Y. Gao, Z. Pan, R. Hu, J. Wang, *InfoMat* **2022**, 4, 12359.
- [4] M. Wang, Z. Bai, T. Yang, C. Nie, X. Xu, Y. Wang, J. Yang, S. Dou, N. Wang, *Adv. Energy Mater.* **2022**, 12, 2201585.
- [5] S. Urbonaitė, T. Poux, P. Novák, *Adv. Energy Mater.* **2015**, 5, 1500118.
- [6] R. F. Service, *Science* **2018**, 359, 1080–1081.
- [7] A. Rosenman, E. Markevich, G. Salitra, D. Aurbach, A. Garsuch, F. F. Chesneau, *Adv. Energy Mater.* **2015**, 5, 1500212.
- [8] X. Wang, Y. Qian, L. Wang, H. Yang, H. Li, Y. Zhao, T. Liu, *Adv. Funct. Mater.* **2019**, 29, 1902929.
- [9] H. J. Peng, J. Q. Huang, X. B. Cheng, Q. Zhang, *Adv. Energy Mater.* **2017**, 7, 1700260.
- [10] Y. Fu, A. Manthiram, *RSC Adv.* **2012**, 2, 5927.
- [11] Q. Du, A. Fox, L. Reinders, K. Küster, T. Acartürk, U. Starke, M. R. Buchmeiser, *ACS Appl. Polym. Mater.* **2023**, 5, 5238–5245.
- [12] H. Raza, S. Bai, J. Cheng, S. Majumder, H. Zhu, Q. Liu, G. Zheng, X. Li, G. Chen, *Electrochem. Energy R.* **2023**, 6 (29), 1–65.
- [13] Q. Du, M. Benedikter, K. Küster, T. Acartürk, U. Starke, J. L. Hoslauer, T. Schleid, M. R. Buchmeiser, *Batter. Supercaps* **2022**, 5, e202200277.
- [14] Q. Du, A. Fox, M. Benedikter, J. Kappler, K. Küster, T. Acartürk, U. Starke, M. R. Buchmeiser, *ACS Appl. Energy Mater.* **2022**, 5, 7642–7650.
- [15] X. Li, X. Sun, *Adv. Funct. Mater.* **2018**, 28, 1801323.
- [16] S. Li, D. Leng, W. Li, L. Qie, Z. Dong, Z. Cheng, Z. Fan, *Energy Storage Mater.* **2020**, 27, 279–296.
- [17] S. Meini, R. Elazari, A. Rosenman, A. Garsuch, D. Aurbach, *J. Phys. Chem. Lett.* **2014**, 5, 915–918.
- [18] M. A. Pope, I. A. Aksay, *Adv. Energy Mater.* **2015**, 5, 1500124.
- [19] M. Zheng, X. Gao, Y. Sun, K. Adair, M. Li, J. Liang, X. Li, J. Liang, S. Deng, X. Yang, Q. Sun, Y. Hu, Q. Xiao, R. Li, X. Sun, *Small Methods* **2021**, 5, 2100420.
- [20] N. He, L. Zhong, M. Xiao, S. Wang, D. Han, Y. Meng, *Sci. Rep.* **2016**, 6, 33871.
- [21] L. Xue, L. Zeng, W. Kang, H. Chen, Y. Hu, Y. Li, W. Chen, T. Lei, Y. Yan, C. Yang, A. Hu, X. Wang, J. Xiong, C. Zhang, *Adv. Energy Mater.* **2021**, 11, 2100420.
- [22] N. Jayaprakash, J. Shen, S. S. Moganty, A. Corona, L. A. Archer, *Angew. Chem. Int. Ed.* **2011**, 50, 5904–5908.
- [23] A. Manthiram, Y. Fu, S.-H. Chung, C. Zu, Y.-S. Su, *Chem. Rev.* **2014**, 114, 11751–11787.

- [24] J. Guo, J. Zhang, F. Jiang, S. Zhao, Q. Su, G. Du, *Electrochim. Acta* **2015**, *176*, 853–860.
- [25] S. Wei, H. Zhang, Y. Huang, W. Wang, Y. Xia, Z. Yu, *Energy Environ. Sci.* **2011**, *4*, 736.
- [26] Y. Zheng, S. Zheng, H. Xue, H. Pang, *J. Mater. Chem. A* **2019**, *7*, 3469–3491.
- [27] B. Duan, W. Wang, A. Wang, K. Yuan, Z. Yu, H. Zhao, J. Qiu, Y. Yang, *J. Mater. Chem. A* **2013**, *1*, 13261.
- [28] H. Kang, H. Kim, M. J. Park, *Adv. Energy Mater.* **2018**, *8*, 1802423.
- [29] Z. W. Seh, H. Wang, P.-C. Hsu, Q. Zhang, W. Li, G. Zheng, H. Yao, Y. Cui, *Energy Environ. Sci.* **2014**, *7*, 672.
- [30] J. Wang, J. Yang, J. Xie, N. Xu, *Adv. Mater.* **2002**, *14*, 963–965.
- [31] M. D. Donohue, G. L. Aranovich, *Adv. Colloid Interface Sci.* **1998**, *76*–*77*, 137–152.
- [32] A. Beda, C. Vaulot, F. Rabuel, M. Morcrette, C. Matei Ghimeau, *Energy Adv.* **2022**, *1*, 185–190.
- [33] C. Bommier, W. Luo, W.-Y. Gao, A. Greaney, S. Ma, X. Ji, *Carbon* **2014**, *76*, 165–174.
- [34] J. Jamnik, J. Maier, *Phys. Chem. Chem. Phys.* **2003**, *5*, 5215.
- [35] J. Zhang, J. Qiao, K. Sun, Z. Wang, *Particuology* **2022**, *61*, 18–29.
- [36] A. M. Awwad, N. M. Salem, A. O. Abdeen, *Adv. Mater. Lett.* **2015**, *6*, 432–435.
- [37] S. Suárez-Gómez, L. Bonavera, J. Carballido-Landeira, P. Blanco, F. Blanco, M. L. Sánchez, F. J. D. Cos, *J. Mater. Res. Technol.* **2020**, *9*, 8117–8124.
- [38] S. Murugan, S. Niesen, J. Kappler, K. Küster, U. Starke, M. R. Buchmeiser, *Batter. Supercaps* **2021**, *4*, 1636–1646.
- [39] L. B. Canto, G. L. Mantovani, E. R. Deazevedo, T. J. Bonagamba, E. Hage, L. A. Pessan, *Polym. Bull.* **2006**, *57*, 513–524.
- [40] E. Frank, E. Muks, A. Ota, T. Herrmann, M. Hunger, M. R. Buchmeiser, *Macromol. Mater. Eng.* **2021**, *306*, 2100280.
- [41] N. Sapkota, S. Chiluwal, P. Parajuli, A. Rowland, R. Podila, *Adv. Sci.* **2023**, *10*, 2206901.
- [42] S. Murugan, S. V. Klostermann, P. Schützendübe, G. Richter, J. Kästner, M. R. Buchmeiser, *Adv. Funct. Mater.* **2022**, *32*, 2201191.
- [43] M. Boota, C. Chen, K. L. Van Aken, J. Jiang, Y. Gogotsi, *Nano Energy* **2019**, *65*, 104022.
- [44] J. Wang, J. Polleux, J. Lim, B. Dunn, *J. Phys. Chem. C* **2007**, *111*, 14925–14931.
- [45] M. Forghani, S. W. Donne, *J. Electrochem. Soc.* **2018**, *165*, A664–A673.
- [46] J. Liu, J. Wang, C. Xu, H. Jiang, C. Li, L. Zhang, J. Lin, Z. X. Shen, *Adv. Sci.* **2018**, *5*, 1700322.
- [47] S. Muduli, R. Das Chakraborty, P. Verma, S. K. Martha, *J. Electrochem. Soc.* **2022**, *169*, 090517.
- [48] S. Muduli, S. K. Pati, T. K. Pani, S. K. Martha, *J. Energy Storage* **2023**, *66*, 107339.
- [49] S. Ghosh, V. Kiran Kumar, S. K. Kumar, S. Biswas, S. K. Martha, *Electrochim. Acta* **2019**, *316*, 69–78.
- [50] J. S. Horner, G. Whang, D. S. Ashby, I. V. Kolesnichenko, T. N. Lambert, B. S. Dunn, A. A. Talin, S. A. Roberts, *ACS Appl. Energy Mater.* **2021**, *4*, 11460–11469.
- [51] A. Nickol, T. Schied, C. Heubner, M. Schneider, A. Michaelis, M. Bobeth, G. Cuniberti, *J. Electrochem. Soc.* **2020**, *167*, 090546.
- [52] W. Weppner, R. A. Huggins, *J. Electrochem. Soc.* **1977**, *124*, 1569–1578.
- [53] G. M. Veith, M. Doucet, R. L. Sacci, B. Vacaliuc, J. K. Baldwin, J. F. Browning, *Sci. Rep.* **2017**, *7* (6326), 1–15.
- [54] C. Xu, F. Lindgren, B. Philippe, M. Gorgoi, F. Björefors, K. Edström, T. Gustafsson, *Chem. Mater.* **2015**, *27*, 2591–2599.
- [55] R. Betancourt-Galindo, P. Y. Reyes-Rodriguez, B. A. Puente-Urbina, C. A. Avila-Orta, O. S. Rodríguez-Fernández, G. Cadenas-Pliego, R. H. Lira-Saldivar, L. A. García-Cerda, *J. Nanomater.* **2014**, *2014*, 1–5.
- [56] G.-B. Cho, J.-P. Noh, H.-J. Sung, S.-H. Lee, Y.-M. Im, H.-J. Ahn, K.-W. Kim, *Nanoscale Res. Lett.* **2012**, *7*, 20.
- [57] J. Fanous, M. Wegner, J. Grimminger, M. Rolff, M. B. M. Spera, M. Tenzer, M. R. Buchmeiser, *J. Mater. Chem. A* **2012**, *22*, 23240.
- [58] S. V. Klostermann, J. Kappler, A. Waigum, M. R. Buchmeiser, A. Köhn, J. Kästner, *Phys. Chem. Chem. Phys.* **2024**, *26*, 9998–10007.

Manuscript received: July 19, 2024

Revised manuscript received: August 11, 2024

Accepted manuscript online: August 23, 2024

Version of record online: October 21, 2024